The Transfinite Element Method for Modeling MMIC Devices

ZOLTAN J. CENDES, MEMBER, IEEE, AND JIN-FA LEE

Abstract—**A new numerical procedure called the transfinite element method is employed in conjunction with the planar waveguide model to analyze MMIC devices. By using analytic basis functions together with finite element approximation functions in a variational technique, the transfinite element method is able to determine the fields and scattering parameters for a wide variety of stripline and microstrip devices. With minor modification, the transfinite element method can also be applied to waveguide junctions. We show that the transfinite element method can be used to treat singular points in waveguide junctions very efficiently. Examples that have been calculated by this method are a rectangular waveguide two-slot-20 dB coupler, stripline band-elimination filter, and several microstrip discontinuity problems. Good agreement of the numerical results with published values demonstrates the validity of the proposed procedure.**

I. Introduction

TO BE USEFUL at high frequencies, models of MMIC devices must solve the wave equations first derived by Maxwell. There are two ways to do this. One way is to solve the full vector wave equations in three-dimensions; the other is to employ the planar circuit model that approximates the fringe fields and hybrid modes of the device but maintains its essential wave and dispersion characteristics. This paper presents a new procedure to solve the second of these alternatives and shows that accurate results are obtained for several typical MMIC devices.

In the planar waveguide model, the scalar Helmholtz equation is solved in two-dimensions for the electromagnetic field distribution. The procedure is as follows [1]–[3]:

1) Approximate the actual three-dimensional MMIC device with an equivalent N-port planar waveguide model.
2) Solve for the electromagnetic fields and scattering matrix coefficients in the equivalent planar waveguide model.

We propose here a new method for the second of these steps that is considerably more efficient and more general than the existing alternatives. The method is based on the transfinite element procedure first proposed by the authors for the solution of unbounded electrostatics problems [4] and later extended to the solution of electromagnetic scattering problems [5]. Unlike the eigensolution procedure reported in [2] that requires that a set of orthonormalized eigenmodes be determined for the planar waveguide, the transfinite element method is deterministic and hence is much more efficient. And, unlike the finite difference time-domain method of [3], the transfinite element method reported here is time harmonic and thus eliminates the need for expensive numerical time integration.

Manuscript received April 14, 1988; revised August 1, 1988. This work was supported in part by the Pennsylvania Ben Franklin Partnership Fund and by the Ansoft Corporation.

The authors are with the Department of Electrical and Computer Engineering, Carnegie Mellon University, Pittsburgh, PA 15213.

IEEE Log Number 8824168.

II. The Planar Waveguide Model

Throughout this paper we will refer to "the equivalent planar waveguide model." In this model the actual three-dimensional MMIC device is transformed into a planar circuit that can be solved by two-dimensional analysis. This is accomplished by replacing the actual dimensions and material properties of the MMIC device with effective dimensions and material properties for an equivalent planar waveguide. This operation is different with striplines than it is with microstrip:

1) In stripline circuits, the dominant propagating mode is TEM, for which effective dimensions are easily calculated by using quasi-static analysis or by using the empirical formula of [1].
2) In microstrip, the dominant mode is non-TEM and the field pattern thus varies with frequency. In the low-frequency limit, the TEM approximation can be used to construct an equivalent planar waveguide model. Formulas that model the frequency dependence of the effective parameters may then be used for higher frequencies.

In this paper, the frequency-dependent effective dielectric constant in the microstrip circuits is given by [10]

$$\epsilon_{re}(f) = \epsilon_r - \frac{\epsilon_r - \epsilon_{re}(0)}{1+P}$$

$$P = \left(\frac{h}{Z_{0m}}\right)^{1.33}\left[0.43f^2 - 0.009f^3\right] \qquad (1)$$

where ϵ_r is the true relative dielectric constant, h is the height of the substrate in millimeters, f is the frequency in GHz, and the characteristic impedance Z_{0m} is in ohms. The frequency-dependent effective width is modeled

as [10]

$$W_e(f) = W + \frac{W_e(0) - W}{1 + f/f_g}$$

$$f_g = \frac{c}{2W\sqrt{\epsilon_r}} \tag{2}$$

where W is the true physical width of the microstrip. The values of the $\epsilon_{re}(0)$ and $W_e(0)$ are calculated by using quasi-static analysis [10]. The accuracy and frequency range of (1), (2) are described fully in [10]. These formulas work well provided that the width of the strip in the discontinuity region is easily determined. However, in some problems the width of the strip is ambiguous and reduces the correctness of this approximation.

III. The Transfinite Element Method

A. The Functional

Fig. 1 shows an equivalent planar waveguide model for a typical MMIC device. Since the fringe field is taken into account by using effective dimensions and material properties, we can write the equation for the component E_z of the electric field perpendicular to the plane of the conductor as

$$\nabla^2 E_z + k^2 \epsilon_{re} E_z = 0 \qquad \text{in } \Omega$$

$$\frac{\partial E_z}{\partial n} = 0 \qquad \text{on } \partial\Omega \tag{3}$$

where Ω is the effective problem domain, $\partial\Omega$ is the boundary on the sides, and ∂n is the normal derivative.

A functional corresponding to (3) is obtained by applying Galerkin's method. The result is

$$F(E_z) = -\int_{\Omega} E_z^* \left(\nabla^2 E_z + k^2 \epsilon_{re} E_z\right) d\Omega \tag{4}$$

where * represents the complex conjugate. We need to separate the solution region into two parts: let Ω_d represent the discontinuity region of the planar circuit, and Ω_i the semi-infinite ports. Equation (4) then becomes

$$F(E_z) = -\int_{\Omega_d} E_z^* \left(\nabla^2 E_z + k^2 \epsilon_{re} E_z\right) d\Omega - \sum_{i=1}^{P} \int_{\Omega_i} E_z^* \left(\nabla^2 E_z + k^2 \epsilon_{re} E_z\right) d\Omega \tag{5}$$

where P is the number of ports. Now apply Green's theorem to the first of these integrals. This gives

$$F(E_z) = \int_{\Omega_d} \left(\nabla E_z^* \cdot \nabla E_z - k^2 \epsilon_{re} E_z^* E_z\right) d\Omega - \sum_{i=1}^{P} \oint_{\Gamma_i} E_z^* \frac{\partial E_z}{\partial n} d\Gamma - \sum_{i=1}^{P} \int_{\Omega_i} E_z^* \left(\nabla^2 E_z + k^2 \epsilon_{re} E_z\right) d\Omega. \tag{6}$$

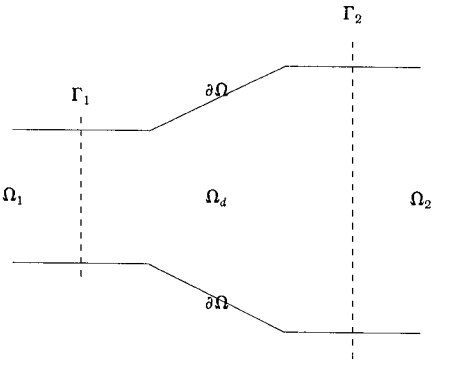

Fig. 1. A two-port planar waveguide junction.

The reason for writing the functional in this form is that the boundary integral in (6) provides the natural boundary conditions for the solution space.

B. The Solution Space

Assume that port 1 is excited by the dominant TEM mode. By modal analysis, the z component of the electric field within port i can be written as

$$E^{(i)} = \delta_{i1}\Phi_{\text{inc}} + \sum_{J=0}^{\infty} a_{iJ}\Phi_{iJ} \tag{7}$$

where δ_{i1} is the Kronecker delta

$$\delta_{i1} = \begin{cases} 1 & \text{if } i = 1 \text{ (input port)} \\ 0 & \text{otherwise} \end{cases} \tag{8}$$

the a_{iJ} are unknown coefficients, and fields Φ_{inc} and Φ_{iJ} are given as

$$\Phi_{\text{inc}} = \exp(\gamma_{10} y)$$

$$\Phi_{iJ} = \cos\left(\frac{j\pi x}{W_i}\right) \exp(-\gamma_{iJ} y). \tag{9}$$

In these equations, W_i is the effective width of port i, and ϵ_{ri} is the effective dielectric constant of port i, and the propagation constant is

$$\gamma_{iJ} = \sqrt{\left(\frac{j\pi}{W_i}\right)^2 - k^2 \epsilon_{ri}}. \tag{10}$$

The local coordinate in port i is defined such that the $+\hat{y}$ direction is the direction of propagation of the scattered wave. The origin of the coordinate is located on the port boundary Γ_i.

The solution space is now taken to be the analytic basis functions (9) for the port regions Ω_i and finite element basis functions for the discontinuity region Ω_d. By separating the finite element nodes in Ω_d into two parts—interior nodes ϕ^I and P sets of boundary nodes ϕ^{Γ_i}, we obtain the

following hybrid solution space:

$$\Lambda \equiv \left\{ \phi | \phi = \begin{cases} \tilde{\alpha}^I \tilde{\phi}^I + \sum_{\iota=1}^{P} \tilde{\alpha}^{\Gamma_\iota} \tilde{\phi}^{\Gamma_\iota} & \text{in } \Omega_d \\ \delta_{\iota 1} \Phi_{\text{inc}} + \sum_{J=0}^{M} a_{\iota J} \Phi_{\iota J} & \text{in } \Omega_\iota \end{cases} \quad \phi \in C^0 \right\} \tag{11}$$

where the α are the Lagrangian interpolation polynomials, $\tilde{}$ denotes a row vector, $\underset{\sim}{}$ denotes a column vector, M is the number of modes in each port, and C^0 is the set of continuous functions. Notice that we have used two different kinds of basis functions in different regions, and also that since the function ϕ must be continuous, these two representations must be matched along the port reference planes.

Since the analytic basis functions satisfy the Helmholtz equation in the port regions, the integral over Ω_ι in (6) is zero, independent of the coefficients $a_{\iota J}$. Thus the functional becomes

$$F(E_z) = \int_{\Omega_d} \left(\nabla E_z^* \cdot \nabla E_z - k^2 \epsilon_{re} E_z^* E_z \right) d\Omega - \sum_{i=1}^{P} \oint_{\Gamma_\iota} E_z^* \frac{\partial E_z}{\partial n} d\Gamma. \tag{12}$$

Continuity of the electric field is imposed by requiring that the field approximations in Ω_d and in Ω_ι be identical at the finite element nodes along the port boundary Γ_ι. This condition may be expressed as

$$\underset{\sim}{\phi}^{\Gamma_\iota} = \delta_{\iota 1} \underset{\sim}{P}_{\text{inc}} + [P_\iota] \underset{\sim}{a}_\iota \tag{13}$$

Here m is the number of nodes on Γ_ι, ^{T} represents the transpose, and x_i is the coordinate of node i.

Note that continuity of the derivative of the electric field is automatically provided by the natural boundary conditions of the functional (6).

C. Extremizing the Functional

By requiring that the trial functions E_z be in the solution space Λ, the boundary integral in (12) can be integrated analytically. The result is

$$\oint_{\Gamma_\iota} E_z^* \frac{\partial E_z}{\partial n} d\Gamma = \delta_{\iota 1} \gamma_{10} a_{10}^* W_1 - \tilde{a}_\iota^* [\gamma_\iota] \underset{\sim}{a}_\iota \tag{15}$$

where

$$[\gamma_\iota]_{jk} = \begin{cases} 0 & j \neq k \\ W_\iota \gamma_{\iota 0} & j = k = 0 \\ W_\iota \gamma_{\iota J}/2 & j = k \neq 0. \end{cases} \tag{16}$$

Finally, substituting (13)–(16) into (12), the functional can then be expressed in matrix form as

$$F(E_z) = \left[\tilde{\phi}^I \underset{\sim}{P}_{\text{inc}} + \tilde{a}_1 [P_1]^T \tilde{a}_2 [P_2]^T \right]^* \cdot \begin{bmatrix} [S_{II}] & [S_{I\Gamma_1}] & [S_{I\Gamma_2}] \\ [S_{\Gamma_1 I}] & [S_{\Gamma_1\Gamma_1}] & [S_{\Gamma_1\Gamma_2}] \\ [S_{\Gamma_2 I}] & [S_{\Gamma_2\Gamma_1}] & [S_{\Gamma_2\Gamma_2}] \end{bmatrix} \begin{bmatrix} \underset{\sim}{\phi}^I \\ \underset{\sim}{P}_{\text{inc}} + [P_1] \underset{\sim}{a}_1 \\ [P_2] \underset{\sim}{a}_2 \end{bmatrix} - a_{10}^* W_1 \gamma_{10} + \sum_{\iota=1}^{P} \tilde{a}_\iota^* [\gamma_\iota] \underset{\sim}{a}_\iota$$

where

$$[S_{\iota J}] = \int_{\Omega_d} \left(\nabla \tilde{\alpha}^\iota \cdot \nabla \underset{\sim}{\alpha}^J - k^2 \epsilon_{re} \tilde{\alpha}^\iota \underset{\sim}{\alpha}^J \right) d\Omega. \tag{17}$$

This equation is shown for clarity with only two ports; if there are more ports, then additional terms similar to that of port 2 need to be added.

Extremizing this with respect to ϕ^{*I} and a_i^* gives the final matrix equation

$$\begin{bmatrix} [S_{II}] & [S_{I\Gamma_1}][P_1] & [S_{I\Gamma_2}][P_2] \\ [P_1]^T [S_{\Gamma_1 I}] & [P_1]^T [S_{\Gamma_1\Gamma_1}][P_1] + [\gamma_1] & [P_1]^T [S_{\Gamma_1\Gamma_2}][P_2] \\ [P_2]^T [S_{\Gamma_2 I}] & [P_2]^T [S_{\Gamma_2\Gamma_1}][P_1] & [P_2]^T [S_{\Gamma_2\Gamma_2}][P_2] + [\gamma_2] \end{bmatrix} \begin{bmatrix} \underset{\sim}{\phi}^I \\ \underset{\sim}{a}_1 \\ \underset{\sim}{a}_2 \end{bmatrix} = \begin{bmatrix} [S_{I\Gamma_1}] \underset{\sim}{P}_{\text{inc}} \\ [P_1]^T [S_{\Gamma_1\Gamma_1}] \underset{\sim}{P}_{\text{inc}} + \gamma_{10} W_1 \underset{\sim}{\delta} \\ [P_2]^T [S_{\Gamma_2\Gamma_1}] P_{\text{inc}} \end{bmatrix} \tag{18}$$

where

$$\underset{\sim}{P}_{\text{inc}} = [1 \quad 1 \quad \cdots \quad 1]^T$$

$$[P_\iota] = [\underset{\sim}{P}_{\iota 0} \quad \underset{\sim}{P}_{\iota 1} \quad \cdots \quad \underset{\sim}{P}_{\iota M}]$$

$$\underset{\sim}{P}_{\iota J} = \left[\cos\left(\frac{j\pi x_1}{W_\iota} \right) \quad \cos\left(\frac{j\pi x_2}{W_\iota} \right) \quad \cdots \quad \cos\left(\frac{j\pi x_m}{W_\iota} \right) \right]^T$$

$$\underset{\sim}{a}_\iota = [a_{\iota 0} \quad a_{\iota 1} \quad \cdots \quad a_{\iota M}]^T. \tag{14}$$

where

$$\underset{\sim}{\delta} = [1 \quad 0 \quad 0 \quad \cdots \quad 0]^T.$$

Notice that since the $[S_{ij}]$ submatrices are sparse and the number of modes M required in the formulation is small, the matrix multiplications in (18) can be done very efficiently. The finally matrix equation is sparse and symmetric and can be solved by using the preconditioned conjugate gradient method (PCCG) [12].

D. The Scattering Matrix

The scattering matrix for two-port circuits is obtained in two steps

1) Take port 1 to be the input port and solve (18). Since the incident wave is assumed to have unit amplitude, the scattering coefficients are defined as

$$S_{11} = a_{10}$$
$$S_{12} = a_{20}\sqrt{\frac{\gamma_{20}W_2}{\gamma_{10}W_1}}. \tag{19}$$

2) Change the input port to be port 2 and repeat the procedure in step 1. The scattering coefficients S_{21}, S_{22} can then be found again by using (19).

For an N-port circuit, the analysis needs to be performed N times to determine the $N \times N$ scattering matrix. From the solution of (18), one obtains not only the scattering matrix of the device but also the excitations of the higher modes on the port reference plane for each port. Chu and Itoh [11] have defined a generalized scattering matrix to characterize microstrip step discontinuities. With the present method, a generalized scattering matrix can be computed for general MMIC devices.

IV. Numerical Results for MMIC Components

A general purpose computer program has been developed to model MMIC devices using the transfinite element method [8]. To show the validity and generality of the method, we present numerical results for several MMIC devices together with the detailed descriptions of the planar waveguide model that has been used in the analysis.

A. Stripline Band-Elimination Filter

Shown in Fig. 2(a) is a two-port stripline filter with a circular disk. The characteristic impedance of both ports is 50 Ω, the substrate height is $2h = 0.64$ cm and the relative dielectric constant is 2.4. To solve this problem with the transfinite element method, we first convert to the equivalent planar waveguide model with the effective dimensions shown in Fig. 2(b). This geometry is then discretized by using triangular finite elements, and solved by means of the transfinite element method. The transmission coefficient computed by means of this procedure is plotted in Fig. 2(c). As shown, good agreement exists between these results and published experimental data [7]. It should be noted that the curve in Fig. 2(c) was produced by using the adaptive spectral response modeling procedure in [9]. The squares on the abscissa of this graph correspond to the frequencies actually employed in the computation.

We also like to point out that the zero in the transmission coefficient in Fig. 2(c) corresponds to the first resonance of the circular disk. The field intensity at the resonance frequency 2.976 GHz is plotted in Fig. 2(d) to provide more physical insight. It is apparent from the intensity plot that the transmission zero is caused by the orthogonality of the modal distribution and of the TEM field distribution at the output port at resonance.

B. Microstrip Step Discontinuity

Fig. 3(a) shows a microstrip step discontinuity with a substrate height $h = 0.635$ mm and substrate dielectric constant $\epsilon_r = 9.7$. The corresponding planar waveguide model at low frequency is shown in Fig. 3(b) together with the frequency-dependent effective parameters. Since the problem is symmetric, only half of the geometry is used to solve for the scattering coefficients. A comparison of the transmission coefficient computed by transfinite element method and by [14] is given in Fig. 3(c). This figure also gives results computed with the *generalized scattering matrix method* [11]. The discontinuity of S_{11} in the figure is due to the excitation of the second mode in the wider port.

C. Microstrip T-Junction

The microstrip T-junction shown in Fig. 4(a) has a substrate height $h = 0.65$ mm and a substrate dielectric constant $\epsilon_r = 10.1$ The quasi-static analysis to find the planar waveguide model at low frequency requires that we solve the Laplace equation twice; this performed in the following way:

- First, input the cross section of the microstrip line as shown in Fig. 4(b). Then create a finite element mesh as shown in Fig. 4(c) by using the process of the *Delaunay triangulation* [13].
- Assume that the top conductor carries constant current and solve for the magnetic vector potential distribution. The magnetic vector potential contours are shown in Fig. 4(d). From the stored energy of the system we can obtain the inductance $L = 0.3373\mu_0$, where μ_0 is the permeability of free space.
- Compute the capacitance by solving the potential distribution. The capacitance computed is $C = 20.322\epsilon_0$, where ϵ_0 is the permittivity of free space. The equal potential contours are shown in Fig. 4(e).
- The effective parameters at low frequency are given by

$$Z = \sqrt{\frac{L}{C}}$$
$$\epsilon_{re} = \frac{LC}{\epsilon_0\mu_0}$$
$$W_e = \frac{Ch}{\epsilon_{re}\epsilon_0}.$$

The characteristics thus computed are summarized as follows:

$$Z = 48.54\ \Omega$$
$$W_e'(0) = 1.927\ \text{mm}$$
$$\epsilon_{re}(0) = 6.855.$$

Also shown in Fig. 4(a) are the formulas which provide the frequency-dependent effective parameters.

The reflection and transmission coefficients computed from the transfinite element method are compared with the results by Mehran [15]. Good agreement is obtained, as

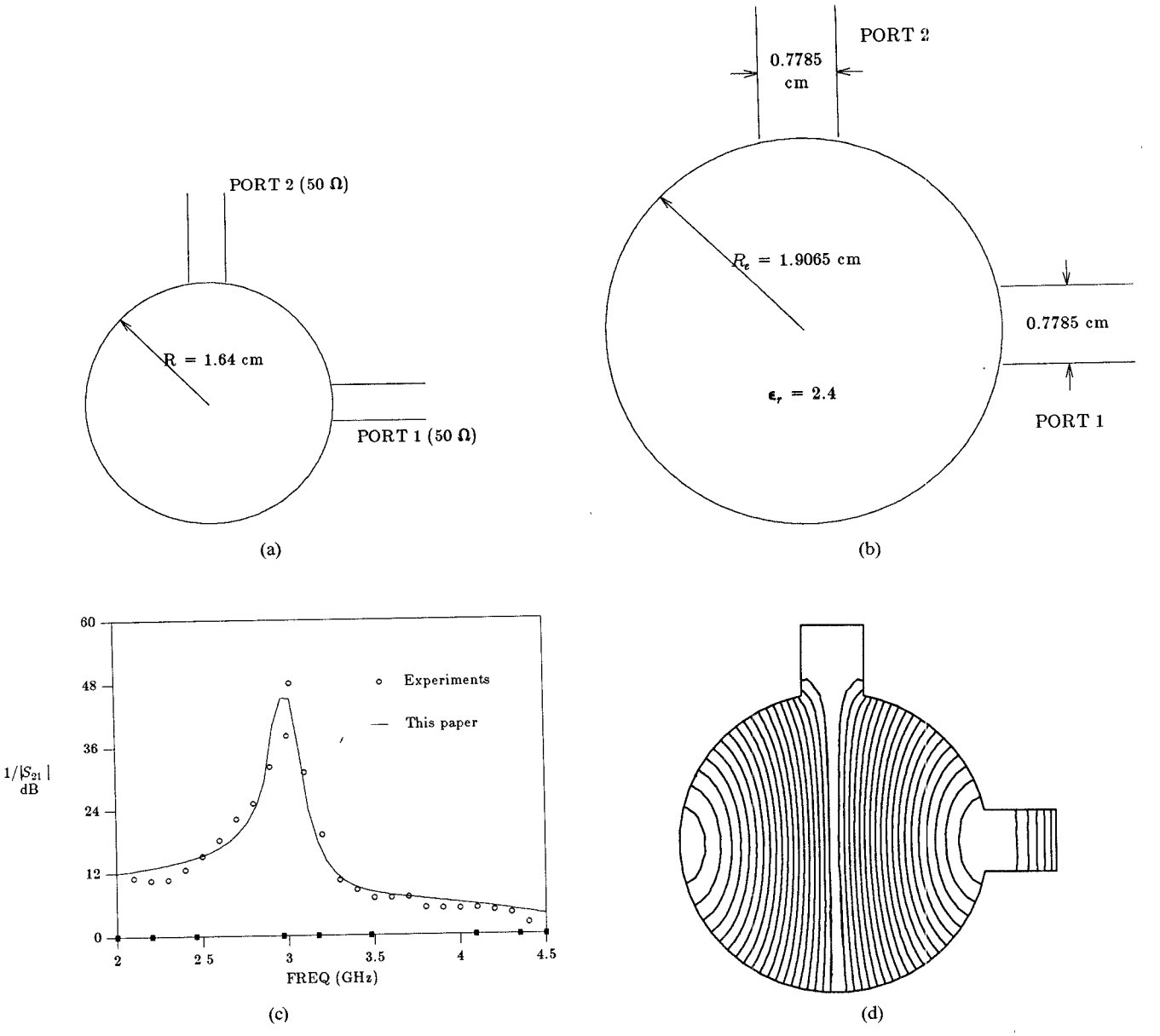

Fig. 2. (a) Geometry of a stripline disk band-elimination filter coupled to two 50 Ω striplines. (b) Planar waveguide model for the stripline disk in (a). (c) Calculation of the transmission coefficient for the band-elimination filter by the transfinite element method compared with experimental values. (d) Contours of equal field intensity for the band-elimination filter at the first transmission zero (2.976 GHz).

can be seen from Fig. 4(f). To understand the transmission zero at 33.7 GHz, we present a plot of the field intensity in Fig. 4(g). A TEM wave comes in from port 1 and excites the first resonance mode in the square region. Because of the TEM excitation in port 1, the polarization is a *cosine* distribution along ports 2 and 3, which are orthogonal to the TEM mode for output.

D. Microstrip Radial Stubs

Fig. 5(a) presents the geometry of a shunt-connected microstrip radial stub. This device has been analyzed by Giannini [16]; we used the formulas from [16] to construct the low-frequency planar waveguide model given in Fig. 5(b). Again, due to the symmetry only one-half of the geometry is modeled. The effective dielectric constant of the radial stub is obtained by using the filling factor for a circular disk capacitor as developed in [17]. Fig. 5(c) shows the finite element mesh with 342 unknowns that is used to obtain the results in Fig. 5(d).

The numerical results in Fig. 5(d) are computed using the model in Fig. 5(b) through the entire frequency range. This neglects the dispersion caused by the effective parameter changes in the microstrip structure. When compared to the measurements in [16], larger discrepancies at high frequencies are observed, although the results are still acceptable. Fig. 5(e) shows the plots of the real part of the field at 3, 7, 11, and 19 GHz. These plots again provide physical insight of the transmission zeros and total transmission in Fig. 5(d). The typical computation time to obtain the response at one frequency for Fig. 5(d) is less than 30 s on a Sun 3/110 workstation.

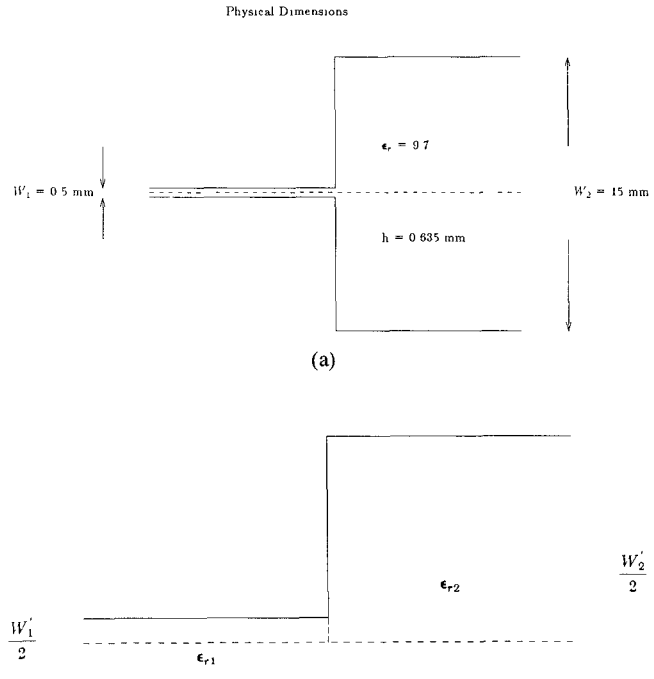

Parameter values

$$Z_1 = 46.94\Omega \qquad Z_2 = 4.655\Omega$$

$$\epsilon_{r1}(f) = 9.7 - \frac{3.3657}{1.0 + 0.00327\left(0.43f^2 - 0.009f^3\right)}$$

$$\epsilon_{r2}(f) = 9.7 - \frac{0.768}{1.0 + 0.0707\left(0.43f^2 - 0.009f^3\right)}$$

$$W_1'(f) = 0.5 + \frac{1.524}{1.0 + \frac{f}{96.324}}$$

$$W_2'(f) = 1.5 + \frac{2.185}{1.0 + \frac{f}{3.211}}$$

(b)

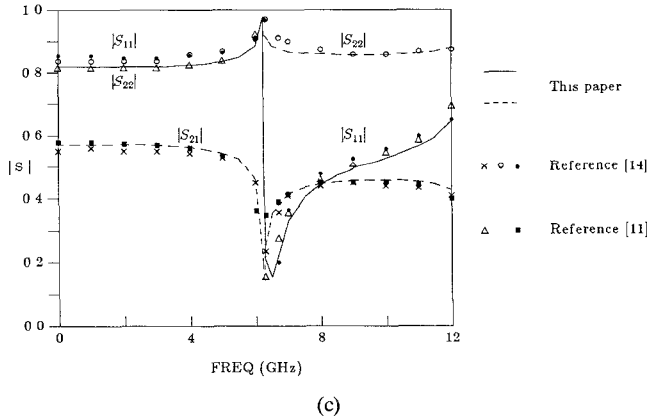

(c)

Fig. 3. (a) Microstrip step discontinuity with a substrate height $h = 0.15$ cm. (b) The planar waveguide model for the step discontinuity and the frequency-dependent effective parameters. (c) Comparison of the scattering coefficients computed by using the transfinite element method for the device in (a) with data from [14] and [11].

E. Waveguide Junction Problems

By changing the analytic basis functions in (9) from a *cosine* to a *sine* distribution within the waveguide regions, the transfinite element method is transformed into a method to model two-dimensional rectangular waveguide junctions. An example of a waveguide junction problem is the rectangular waveguide two-slot coupler shown in Fig. 6(a). The coupling of the incident wave to ports 2 and 4 are through the apertures. The current density at the edges of the slots are mathematically infinite and are called singular points.

The usual approach to model singular points with finite elements is to use more elements around the point as shown in Fig. 6(b). The total number of unknowns for the mesh shown in Fig. 6(b) is 492, and the scattering coefficients computed by the transfinite element method are plotted in Fig. 6(c), together with measured data [6]. A large discrepancy between the computed data and the measurements exists, as can be seen from the figure. In order to improve the accuracy of the numerical model at singular points, we introduce the use of transfinite singular elements.

F. Singular Elements

In Fig. 6(d) we show two conducting planes that intersect at an angle β. When $\beta > \pi$, the field becomes singular at this point. Notice in the figure that we can enclose the singular point with a circular arc with radius r_0. If the radius r_0 is much smaller than the wavelength, the Helmholtz equation can be replaced by the Laplace equation within the circular region. Hereafter, we will refer to the circular region as the *singular region* Ω_s. From [18], the electric field in the singular region can then be written as

$$E(\rho, \theta) = e_1 \rho^{\pi/\beta} \sin\left(\frac{\pi\theta}{\beta}\right) \tag{20}$$

where ρ is the distance from the singular point, θ is the angle, and e_1 is an unknown coefficient. We have found that using even the single basis function in (20) in the transfinite element method is enough to model the solution in the singular region Ω_s.

Along the lines of the previous sections, we divide the problem domain for the waveguide junction with singularities into three parts: a discontinuity region Ω_d, waveguide regions Ω_t, and singular regions Ω_s. Accordingly, the solution space in (11) becomes

$$\Lambda \equiv \left\{ \phi \mid \phi = \begin{cases} \tilde{\alpha}^I \phi^I + \sum_{t=1}^{P} \tilde{\alpha}^{\Gamma_t} \phi^{\Gamma_t} + \tilde{\alpha}^{\Gamma_s} \phi^{\Gamma_s} & \text{in } \Omega_d \\ \delta_{tI} \Phi_{\text{inc}} + \sum_{J=0}^{M} a_{tJ} \Phi_{tJ} & \text{in } \Omega_t \quad \phi \in C^0 \\ e_1 \rho^{\pi/\beta} \sin\left(\frac{\pi\theta}{\beta}\right) & \text{in } \Omega_s \end{cases} \right\}. \tag{21}$$

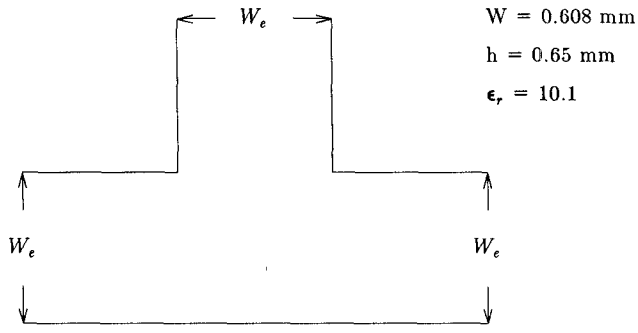

Planar Waveguide Model :

$$Z=48.54\Omega$$

$$W'(f)=0.608+\frac{1.319}{1.0+\frac{f}{77.6295}}$$

$$\epsilon_{re}(f)=10.1-\frac{3\ 245}{1.0+0.00307\left(0.43f^2-0.009f^3\right)}$$

(a)

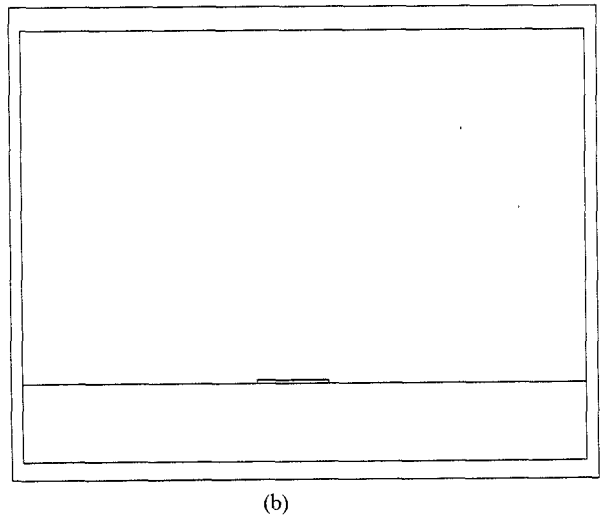

(b)

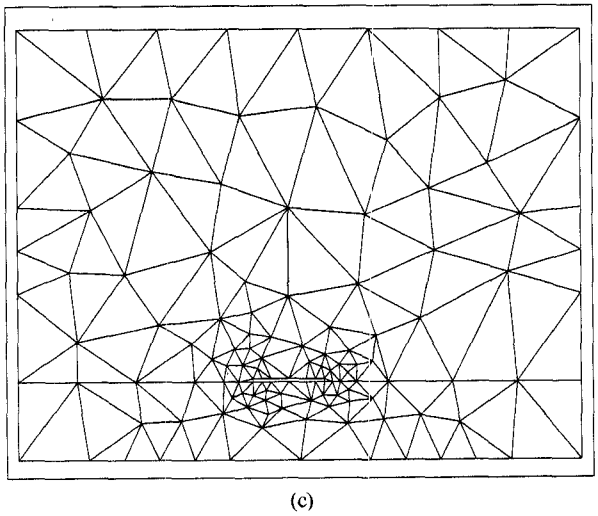

(c)

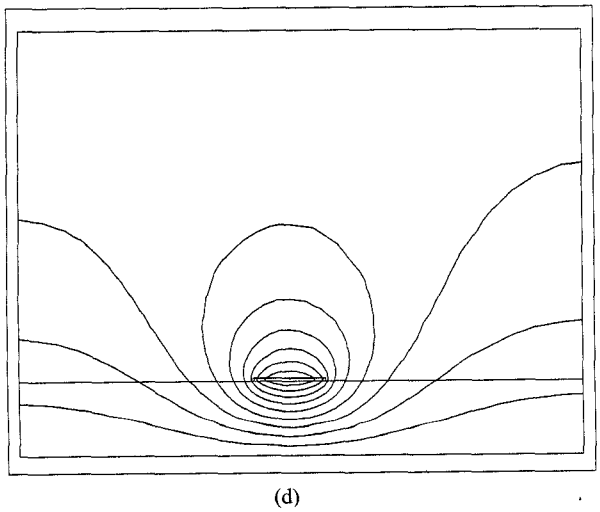

(d)

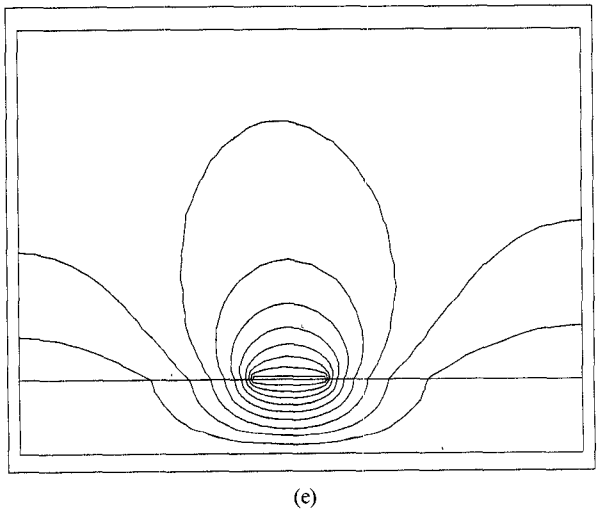

(e)

Fig. 4. (a) A microstrip T-junction with equal field impedance in all ports and the corresponding planar waveguide model. (b) Cross section of the microstrip line. (c) The Delaunay triangulation of (b). (d) Equal magnetic vector potential contours for inductance calculation. (e) Equal potential contours with dielectric constant $\epsilon_r = 10.1$ for capacitance calculation (*continued*).

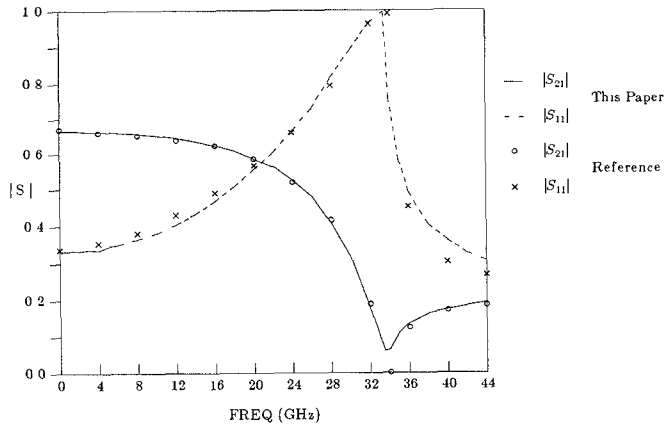

(f)

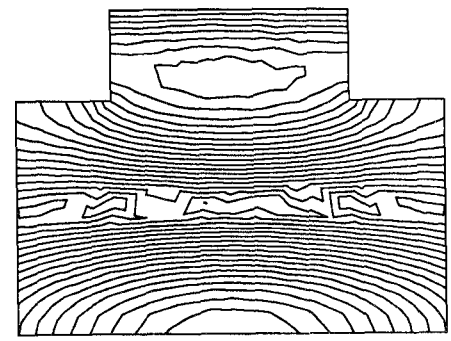

(g)

Fig. 4. (*Continued*) (f) Numerical results for the reflection and the transmission coefficients for the T-junction compared with Mehran [15]. (g) Contours of equal field intensity for the T-junction at 33.7 GHz.

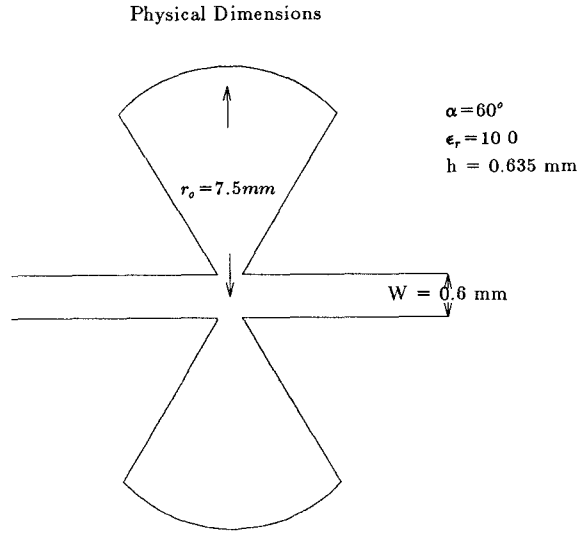

(a)

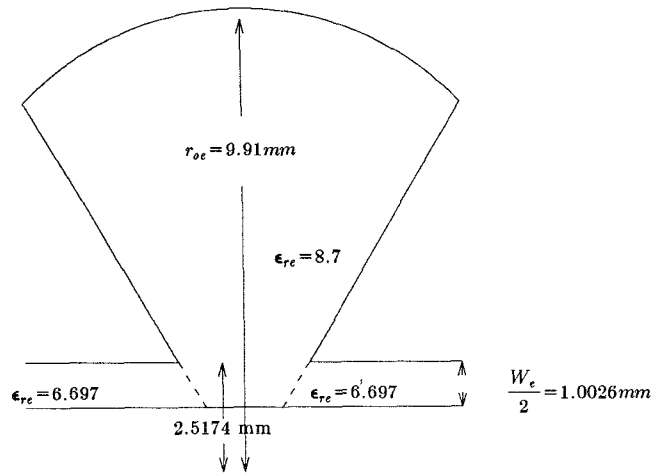

(b)

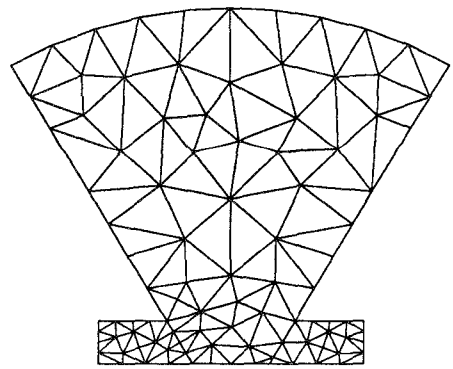

(c)

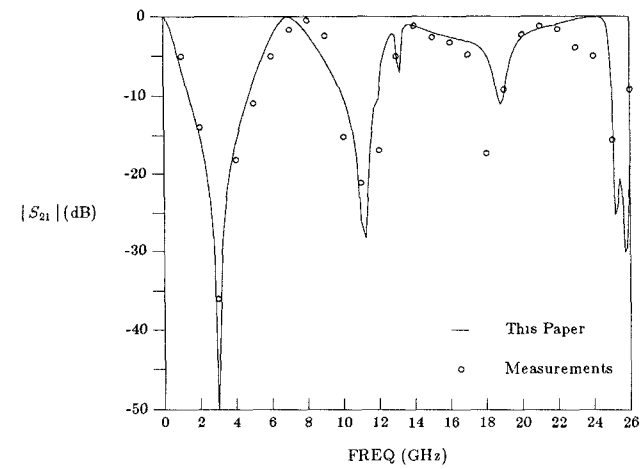

(d)

Fig. 5 (a) Geometry of a shunt-connected microstrip radial stub. (b) The planar waveguide model of the radial stub at low frequency for (a) (c) Finite element mesh for the microstrip radial stub. (d) Comparison of the computed $|S_{21}|$ for the radial stub with the experimental data in [16] (*continued*).

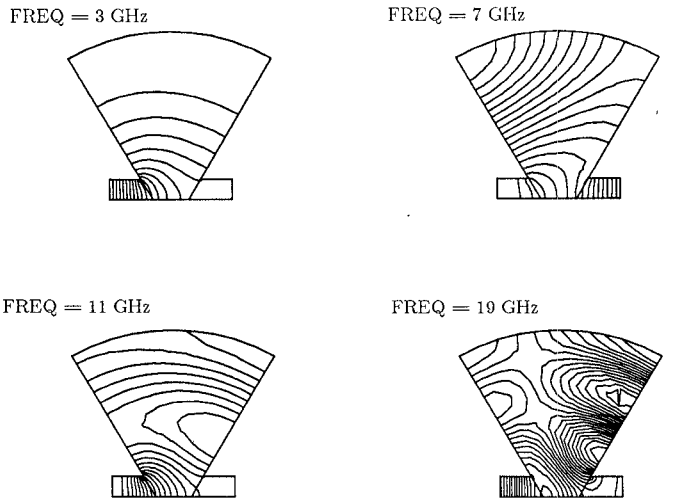

(e)

Fig. 5. (*Continued*) (e) Plots of the real part of the field at 3, 7, 11, and 19 GHz.

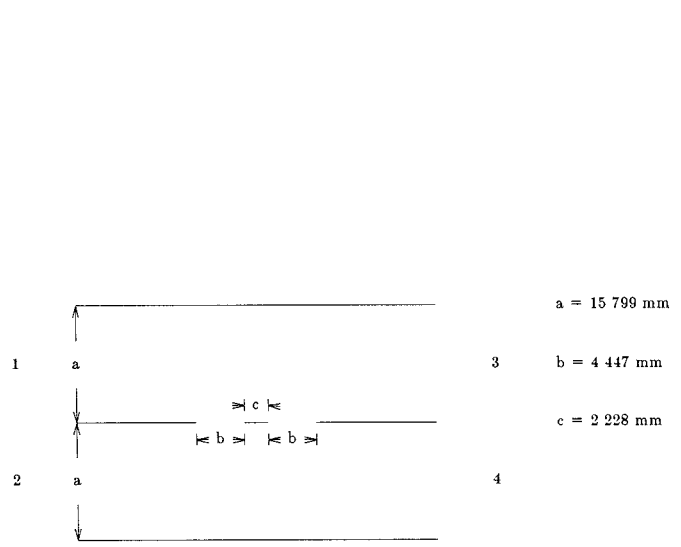

(a)

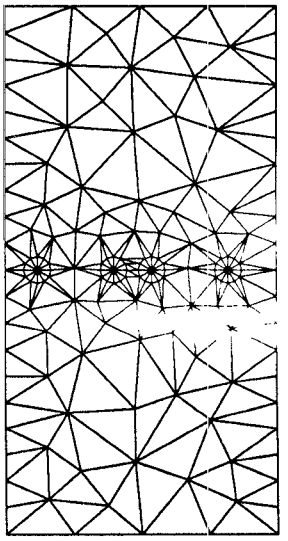

(b)

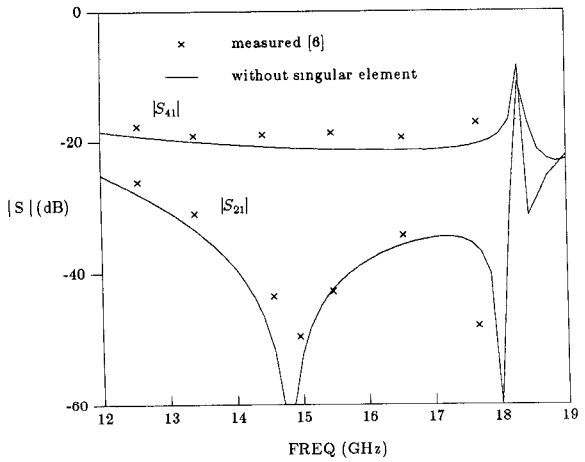

(c)

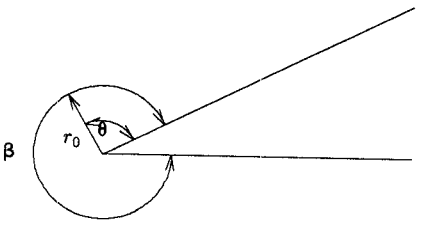

(d)

Fig. 6. (a) A waveguide two-slot −20 dB coupler. (b) Finite element mesh for the waveguide coupler with local mesh refinement. (c) Results computed by the transfinite element method without employing singular elements compared to measurements [6]. (d) A typical singular point (*continued*).

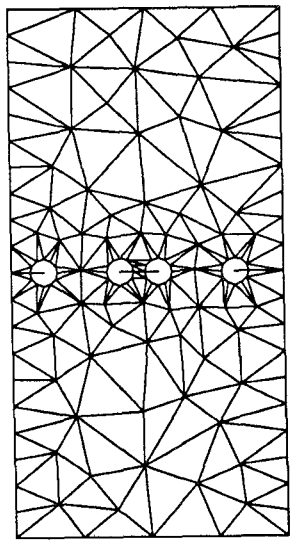

(e)

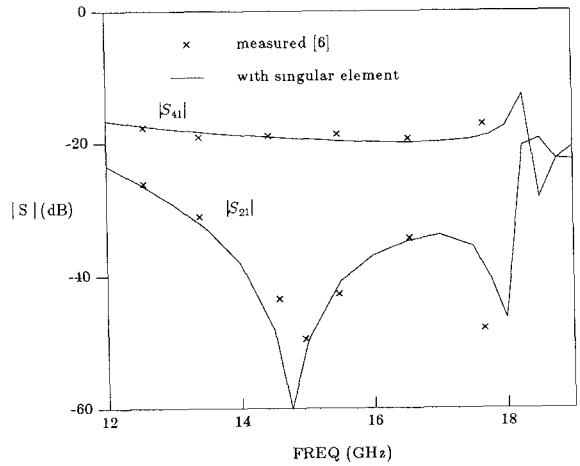

(f)

Fig. 6. (*Continued*) (e) Finite element mesh with singular elements. (f) Comparison of the results from the transfinite element method that includes singular elements with measurements [6].

Notice that the finite element nodes have been separated into: interior nodes ϕ^I, boundary nodes ϕ^{Γ_i} on port reference plane i, and boundary nodes ϕ^{Γ_s} along the circular arc Γ_s.

The functional becomes

$$F(E_z) = \int_{\Omega_d} \left(\nabla E_z^* \cdot \nabla E_z - k^2 \epsilon_{re} E_z^* E_z\right) d\Omega - \sum_{i=1}^{P} \oint_{\Gamma_i} E_z^* \frac{\partial E_z}{\partial n} d\Gamma - \oint_{\Gamma_s} E_z^* \frac{\partial E_z}{\partial n} d\Gamma. \quad (22)$$

The new boundary integral in the functional may be integrated analytically to give

$$\oint_{\Gamma_s} E_z^* \frac{\partial E_z}{\partial n} d\Gamma = e_1^* r_0^{2\pi/\beta} \frac{\beta}{2} e_1. \quad (23)$$

Finally, imposing continuity conditions and performing the variational analysis as in the previous sections, we obtain a singular element to model waveguide junction discontinuities.

G. Scattering Coefficients Computed by Using the Singular Element

Fig. 6(e) shows the finite element mesh for the problem in Fig. 6(a) using singular elements at the slot edges. The total number of unknowns is 362 since the singular element requires fewer basis functions to model the singularity. The computed scattering coefficients S_{21}, S_{41} are plotted in Fig. 6(f). Compared to experimental values [6], much more accurate answers are obtained by using singular elements than is the case with conventional elements.

V. Conclusion

A new numerical procedure has been developed that employs the planar waveguide model to analyze passive MMIC devices. Various components have been studied using the new method and the results compared with previously published methods or experimental data; good agreement is observed in many cases. The method has also been applied to model arbitrary waveguide discontinuity problems. In these cases, a singular element has been developed to model the infinite fields that occur at reentrant corners.

Acknowledgment

The authors would like to express their thanks to Dr. D. Sun for stimulating discussion.

References

[1] T. Okoshi and T. Miyoshi, "The planar circuit—An approach to microwave integrated circuitry," *IEEE Trans. Microwave Theory Tech.*, vol. MTT-20, pp. 245–252, Apr. 1972.

[2] R. Sorrentino, "Planar circuits, waveguide models, and segmentation method," *IEEE Trans. Microwave Theory Tech.*, vol. MTT-33, pp. 1057–1066, Oct. 1985.

[3] W. K. Gwarek, "Analysis of an arbitrarily-shaped planar circuit—A time-domain approach," *IEEE Trans. Microwave Theory Tech.*, vol. MTT-33, pp. 1067–1072, Oct. 1985.

[4] J. F. Lee and Z. J. Cendes, "Transfinite elements: A highly efficient procedure for modeling open field problems," *J. Appl. Phys.*, vol. 61, pp. 3913–3915, Apr. 1987.

[5] J. F Lee and Z. J. Cendes, "The transfinite element method for computing electromagnetic scattering from arbitrary lossy cylinders," *IEEE AP-S International Symposium Digest*, AP03–5, pp. 99–102, June 1987.

[6] H. Schmiedel and F. Arndt, "Field theory design of rectangular waveguide multiple-slot narrow-wall couplers," *IEEE Trans. Microwave Theory Tech.*, vol. MTT-34, pp. 791–797, July 1986.

[7] R. R. Bonetti and P Tissi, "Analysis of planar disk networks," *IEEE Trans. Microwave Theory Tech.*, vol. MTT-26, pp. 471–477, July 1978.

[8] *Maxwell Microwave IC Computer Program Users Guide*, Ansoft Corp., Pittsburgh, PA, 1987

[9] J. F. Lee and Z. J. Cendes, "An adaptive spectral response modeling procedure for multi-port microwave circuits," *IEEE Trans. Microwave Theory Tech.*, vol MTT-35, pp. 1240–1247, Dec. 1987.

[10] K. C. Gupta, R. Garg, and I. J. Bahl, *Microstrip Lines and Slotlines*. Norwood, MA: Artech House, 1979.

[11] T. S. Chu and T Itoh, "Generalized scattering matrix method for analysis of cascaded and offset microstrip step discontinuities,"

IEEE Trans. Microwave Theory Tech., vol. MTT-34, pp. 280–284, Feb. 1986.
[12] M. Hestenes, *Conjugate Direction Methods in Optimization*. New York: Springer–Verlag, 1980.
[13] Z. J. Cendes, D. N. Shenton, and H. Shahnasser, "Magnetic field computation using Delaunay triangulation and complementary finite element methods," *IEEE Trans. Magn.*, vol. MAG-19, pp. 2551–2554, 1983.
[14] G. Kompa, "S-matrix computation of microstrip discontinuities with a planar waveguide model," *Arch. Elek. Übertragung.*, vol. 30, pp. 58–64, Feb. 1976.
[15] R. Mehran, "Calculation of microstrip bends and Y-junctions with arbitrary angle," *IEEE Trans. Microwave Theory Tech.*, vol. MTT-26, pp. 400–405, June 1978.
[16] F. Giannini, M. Ruggieri, and J. Vrba, "Shunt-connected microstrip radial stubs," *IEEE Trans. Microwave Theory Tech.*, vol. MTT-34, pp. 363–366, Mar. 1986.
[17] I. Wolff and N. Knöppik, "Rectangular and circular microstrip disk capacitors and resonators," *IEEE Trans. Microwave Theory Tech.*, vol. MTT-22, pp. 857–864, Oct. 1974.
[18] J. D. Jackson, *Classical Electrodynamics*. New York: Wiley, 1975, pp. 75–78.

✠

Zoltan J. Cendes (S'67–M'73) was born in Feffernitz, Austria, on May 16, 1946. He received the B.S. degree in science engineering from the University of Michigan in 1968 and the M.S. and Ph.D. degrees in electrical engineering from McGill University in 1970 and 1972, respectively.

From 1974 to 1980, he was with the General Electric Company in Schenectady, NY, where he developed finite element tools for modeling electrostatic, electromechanical, and high-frequency electromagnetic devices. In 1980, he was appointed Associate Professor of Electrical Engineering at McGill University; he joined the Department of Electrical and Computer Engineering at Carnegie Mellon University in 1982, where he is currently Professor. He is also cofounder of the Ansoft Corporation, a supplier of easy-to-use electromagnetics design software.

Dr. Cendes's research interests are to develop flexible CAE tools for electromagnetic design. Current projects include the use of Delaunay tessellation for finite element mesh generation, the development of edge-based finite elements for modeling three-dimensional electromagnetics problems, and the use of artificial intelligence to optimize engineering design parameters. He has published over 80 technical papers and was Director of the IEEE Short Course on Magnetics CAD in 1985 and 1986.

✠

Jin-Fa Lee was born in Taipei, Taiwan, in 1960. He received the B.S. degree in electrical engineering from the National Taiwan University, Taiwan, in 1982 and the M.S. degree in electrical engineering from Carnegie Mellon University in 1986. He is currently a full-time research assistant working toward the Ph.D. degree in electrical engineering at Carnegie Mellon University. His fields of interest include MMIC device modeling, fiber optics, and electromagnetic scattering.